

A thermal bistability-based method for real-time optimization of ultra-low threshold whispering gallery mode microlasers

Guoping Lin^{1,2}, Y. Candela¹, O. Tillement³, Zhiping Cai², V. Lefèvre-Seguin¹ and J. Hare¹

¹Laboratoire Kaster Brossel, ENS, UPMC, CNRS – 24 rue Lhomond, 75231 PARIS cedex 05, France

² Department of Physics, Xiamen University, Xiamen 361005, Fujian, P. R. China

³ LPCML, Université Claude Bernard Lyon 1, 10 rue André-Marie Ampère, 69622 Villeurbanne cedex, France

*Corresponding author: Jean.Hare@lkb.ens.fr

Compiled October 1, 2015

A method based on thermal bistability for ultra-low threshold microlaser optimization is demonstrated. When sweeping the pump laser frequency across a pump resonance, the dynamic thermal bistability slows down the power variation. The resulting lineshape modification enables a real-time monitoring of the laser characteristic. We demonstrate this method for a functionalized microsphere exhibiting a sub-microwatt laser threshold. This approach is confirmed by comparing the results with a step-by-step recording in quasi-static thermal conditions. © 2015 Optical Society of America

OCIS codes: 140.3945, 140.3410, 140.3530, 140.6810, 130.3990

Optical microcavities have drawn a large interest in the last two decades and received numerous applications, including Cavity-QED and photonic devices, like light emitting diodes or microlasers. A special attention has been devoted to whispering gallery mode (WGM) microcavities induced by surface tension, like microspheres and microtoroids. They benefit from the sub-nanometer roughness of molten silica, which results in very high quality factors Q , enabling laser operation with a pump power in the sub-microwatt range [1]. These ultra-low-threshold lasers have been obtained by silica functionalization with embedded rare earth ions. Different doping techniques, like fiber doping, sol-gel coating, ion implantation, co-deposition or co-sputtering have been successfully used with Nd^{3+} , Er^{3+} , and Yb^{3+} or mixtures [1–4].

In this paper, we report on a new method for the fast measurement of the laser light-light characteristic based on thermal effect, and allowing real-time optimization. In monolithic microcavities, self-heating by the minute dissipated optical power induces a negative frequency shift, resulting in a bistable behavior when this shift exceeds the cold cavity linewidth [5–7]. For decreasing laser frequency, the heating pushes cavity resonance frequency in the same direction, and they remain close to resonance, as long as the thermal shift compensates the laser offset. The loss of the resonance results in a rapid drop of the coupling. In reverse direction, the thermal shift and the laser scan have opposite directions, and the line is narrowed. Due to the high- Q and the small heat capacity of the cavity, the bistability threshold is very low, typically in the microwatt range or less. At low scanning rate (typically up to 100 Hz) the heating affects the cavity as a whole, and only one cooling time is involved, while for increasing scanning rate a dynamical thermal effect appears which depends on the heat diffusion details. Our method exploits the low frequency regime, with a decreasing pump frequency so that the resonance shifts in the same direction as the laser.

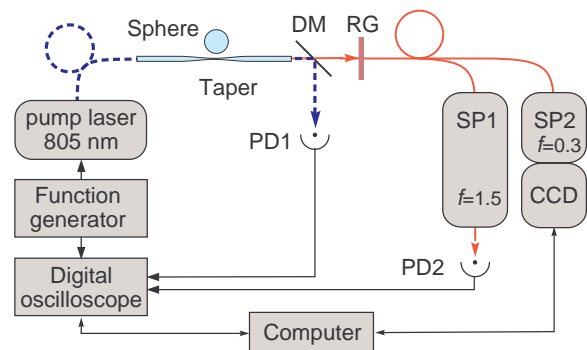


Fig. 1. (Color online) Sketch of the experimental setup. Pump laser and microlaser beams are shown in dotted blue and solid red, respectively. DM: dichroic mirror; RG: Schott filter RG850; SP1&SP2 : spectrometers.

In our experiment, the microlaser is optically pumped by a laser injected in a WGM. In contrast to usual techniques, its frequency is not fixed, but is continuously swept across the resonance, at a nearly constant power. The thermal effect converts this frequency modulation into a smooth sweep of the power coupled into the cavity. The simultaneous monitoring of the injected power and the emitted signal thus directly provides a real-time measurement of the pump-microlaser characteristic, conveniently displayed on an oscilloscope. This method is demonstrated on silica microspheres functionalized with neodymium, which reproducibly feature a sub-microwatt laser threshold. It is shown to be consistent with the results of a more conventional step-by-step method, relying on static thermal effect.

Our experimental setup is sketched in Fig. 1. The microsphere fabrication and the heart of the experiment where the microsphere is evanescently coupled to the fiber taper are explained in [8]. The taper is produced as described in [9].

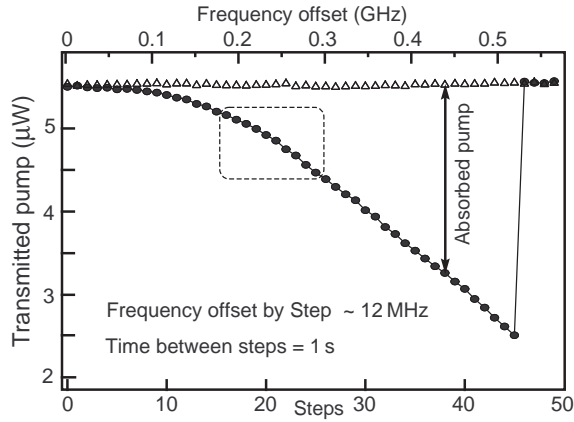


Fig. 2. Transmitted pump vs steps. Empty triangles: reference obtained for a large gap. Full circles: dip observed for a gap of ~ 150 nm. The vertical arrow denotes the “absorbed pump power”. The dotted zone defines the spectra plotted in Fig. 3.

The microspheres are functionalized by dip-coating in an alcoholic colloidal suspension of Nd-doped Gd_2O_3 nanocrystals [10], followed by heating for a few seconds in order to anneal the emitters and to embed them into the sphere. The functionalized microspheres feature Q -factors ranging from 10^7 to 10^8 at pump wavelength $\lambda_p \approx 805$ nm and at least 10^8 at emission wavelength $\lambda_e \approx 1083$ nm. The corresponding Nd content in the WGM volume is below 10 ppm, two orders of magnitude smaller than in [1]. Since aging problems due to water deposition are often observed, the typical $66 \mu\text{m}$ diameter silica microsphere described here was stored for a few days in order to achieve stable lasing conditions. Its Q -factor was reduced to 8.5×10^6 at λ_p and 4.7×10^7 at λ_e . These very high figures lead to low lasing threshold and an even lower thermal bistability threshold.

The pump is a free running laser diode at $\lambda_p \approx 805$ nm, coupled to the fiber taper and tuned to a narrow linewidth and low angular order WGM, selected by the method of [8]. At the taper output, the transmitted pump and the emitted light coupled out by the taper are separated by a dichroic mirror. The transmitted pump is measured by the silicon detector PD1. The emitted light is either filtered using a high resolution (~ 0.01 nm) spectrometer (SP1) and measured with PD2, or analyzed at a lower resolution with a short focal length spectrometer (SP2) equipped with a spectroscopic camera (CCD), providing broadband emission spectra of Nd^{3+} ions.

To establish a firm evidence of laser action and of the threshold value, we present first a step-by-step variant of our method. In this method, the frequency of the pump laser diode is decreased stepwise, at a time rate of about 1 point every 1 s. This time is much longer than the time constants of thermal effect ($\lesssim 15$ ms) and of laser dynamics, such that each step corresponds to a steady-state operation, and to the static thermal bistability condition. In Fig. 2, we plot the transmitted pump intensity (PD1)

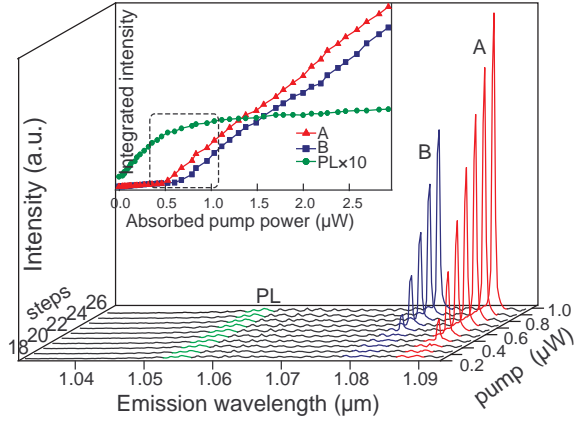


Fig. 3. (Color online) Emission spectra with increasing absorbed pump power for a step range denoted by the dashed rectangle in inset and Fig. 2. Inset: area of peaks A and B and of PL.

as a function of the step number (ie pump frequency). The *absorbed* pump power is given by the absorption dip, obtained by difference between the nearly constant reference measured with uncoupled sphere and the loaded transmission, as shown by the vertical arrow.

Some emission spectra recorded on CCD during this frequency-steeping are plotted in 3-D in Fig. 3. They clearly evidence a bi-mode laser operation with a threshold of about 500 nW. This is confirmed by the inset, where the area of the lasing peaks A and B, and of the 1054 nm photoluminescence (PL), are plotted as a function of the absorbed pump power. The PL clearly exhibits a quasi-saturation at threshold, an expected signature of population clamping.

We now move on to the real-time method. The pump laser is then continuously swept across the WGM resonance, over the same frequency range of ~ 0.6 GHz and the incident pump power is kept lower than $10 \mu\text{W}$ in the whole experiment. We now use SP1 to filter out a *single* emission WGM (peak A in Fig. 3). The transmitted pump intensity measured on PD1 and the filtered laser signal measured on PD2 are simultaneously monitored on a digital oscilloscope, leading to the curves plotted in Fig. 4. In this figure, the pump signal (upper blue curve) exhibits a strong thermal dynamical bistability, characterized by the asymmetry between the decreasing and increasing frequency half-periods. The purple dotted curve is a best fit to the numerical solution of the differential equation for the temperature difference $\theta(t) = T(t) - T_0$:

$$\frac{d\theta}{dt} = \frac{A P_{\text{inc}}}{\Delta^2(t) + (\gamma/2)^2} - \gamma_{th} \theta(t), \quad (1)$$

where the first term, accounting for the heating, is proportional (with a constant A) to the incident power P_{inc} and to a Lorentzian-shaped curve involving the effective detuning $\Delta(t) = \omega(t) - \omega_0 - K\theta(t)$, where $\omega(t)$ is the pump frequency, and K the cavity thermo-optic coefficient. The second term represents the thermal leak. As

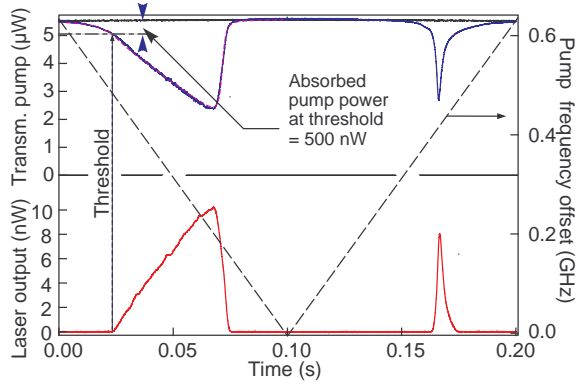


Fig. 4. (Color online) Simultaneous recording of the absorption dip and microsphere emission. Upper curves correspond to transmitted pump power. Black: reference transmission; Blue: absorption dip; Purple dotted: best fit to the theoretical transmission curve deduced from Eq. (1). Lower red: measured laser emission. Dashed black: pump laser frequency offset.

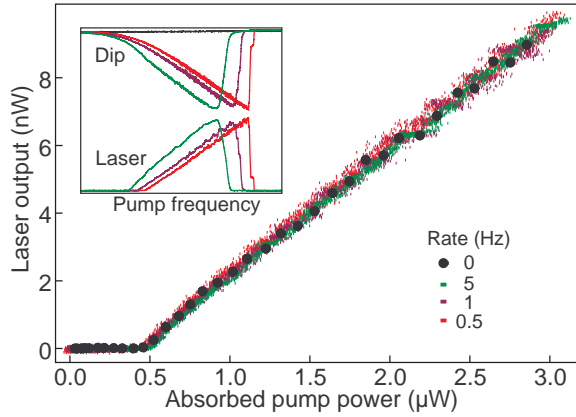


Fig. 5. (Color online) Light-light curve, for different scan speeds. Inset: corresponding transmitted pump and laser output curves.

previously, the baseline (black curve) was recorded with a large coupling gap, and the absorbed pump power is determined by difference with the baseline.

One notices that the onset of microsphere emission occurs later than the start of pump absorption, demonstrating a threshold effect. An X-Y plot, as used in Fig. 5, allows to measure the threshold and estimate the differential efficiency in *real-time*. This method is much quicker and easier to set-up than the standard power sweep and enables an efficient optimization in real-time.

In order to demonstrate the consistency of this method, we swept the pump laser at different repetition frequencies between 0.5 Hz and 25 Hz. The modulation frequency affects the resonance shape, but for slow enough frequencies, the X-Y plot provides the same light-light characteristic, as shown in Fig. 5. In this figure the characteristics obtained for modulations frequencies of 0.5, 1 and 5 Hz are plotted with red, purple, and green dots, respectively. The very good overlap of these

curves demonstrates that the observed threshold and slope efficiency do not depend on the repetition rate. This is no longer true when using higher frequencies (typically above 10 Hz), where an increasing departure (not shown) is observed, mostly due to the weakening of the thermal effect, as we have verified thanks to a numerical simulation based on (1). To fully demonstrate that the observed light-light curve is the same as it would be observed in steady state, we have combined the real-time method with the frequency-steeping described above. By recording at each step the absorbed pump power and the microlaser power transmitted by SP1 on PD2, we have obtained the curve displayed with black circles in Fig. 5, in perfect agreement with the real-time characteristic. It is worth mentioning that this method uses non-steady state thermal effect, while the much faster laser dynamics is nearly in steady-state and can adiabatically follow the temperature and pump power variations.

In summary, we have developed a simple method to characterize the laser characteristic of rare-earth based microlasers, taking advantage of the very high quality factor of the doped microcavities. This results in a strong thermal effect, allowing to control the pump power by the mean of frequency sweeping. This method can work at a rate as high as 10 Hz, allowing a real-time optimization of the coupling conditions. This approach allows to demonstrate a sub-microwatt threshold neodymium-based laser, and will be applied for further optimizations to be published in a near future.

This work has been supported by the Region Île-de-France in the framework of C’Nano IdF (Nanoscience competence center of Paris Region). G.L. acknowledges support from the China Scholarship Council.

References

1. V. Sandoghdar, F. Treussart, J. Hare, V. Lefèvre-Seguin, J.-M. Raimond, and S. Haroche, *Phys. Rev. A* **54**, R1777 (1996).
2. F. Lissillour, P. Feron, N. Dubreuil, P. Dupriez, M. Poulain, and G. M. Stephan, *Electron. Lett.* **36**, 1382 (2000).
3. L. Yang, D. K. Armani, and K. J. Vahala, *Appl. Phys. Lett.* **83**, 825 (2003).
4. E. Ostby, L. Yang, and K. Vahala, *Opt. Lett.* **32**, 2650 (2007).
5. V. B. Braginsky, M. L. Gorodetsky, and V. S. Ilchenko, *Phys. Lett. A* **137**, 393 (1989).
6. H. Rokhsari, S. Spillane, and K. Vahala, *Appl. Phys. Lett.* **85**, 3029 (2004).
7. T. Carmon, L. Yang, and K. Vahala, *Opt. Express* **12**, 4742 (2004).
8. G. Lin, B. Qian, F. Oručević, Y. Candela, J. Jager, Z. Cai, V. Lefèvre-Seguin, and J. Hare, *Opt. Lett.* **35**, 583 (2010).
9. F. Orucevic, V. Lefèvre-Seguin, and J. Hare, *Opt. Express* **15**, 13624 (2007).
10. R. Bazzi, A. Brenier, P. Perriat, and O. Tillement, *J. Lumin.* **113**, 161 (2005).

References

1. V. Sandoghdar, F. Treussart, J. Hare, V. Lefèvre-Seguin, J.-M. Raimond, and S. Haroche, “Very low threshold whispering-gallery mode microsphere laser,” *Phys. Rev. A* **54**, R1777 (1996).
2. F. Lissillour, P. Feron, N. Dubreuil, P. Dupriez, M. Poulain, and G. M. Stephan, “Erbium-doped microspherical lasers at $1.56\ \mu\text{m}$,” *Electron. Lett.* **36**, 1382–1384 (2000).
3. L. Yang, D. K. Armani, and K. J. Vahala, “Fiber-coupled erbium microlasers on a chip,” *Appl. Phys. Lett.* **83**, 825–827 (2003).
4. E. Ostby, L. Yang, and K. Vahala, “Ultralow-threshold $\text{Yb}^{3+}:\text{SiO}_2$ glass laser fabricated by the solgel process,” *Opt. Lett.* **32**, 2650–2652 (2007).
5. V. B. Braginsky, M. L. Gorodetsky, and V. S. Ilchenko, “Quality-factor and non-linear properties of optical whispering-gallery modes,” *Phys. Lett. A* **137**, 393–397 (1989).
6. H. Rokhsari, S. Spillane, and K. Vahala, “Loss characterization in microcavities using the thermal bistability effect,” *Appl. Phys. Lett.* **85**, 3029 (2004).
7. T. Carmon, L. Yang, and K. Vahala, “Dynamical thermal behavior and thermal self-stability of microcavities,” *Opt. Express* **12**, 4742–4750 (2004).
8. G. Lin, B. Qian, F. Oručević, Y. Candela, J. Jager, Z. Cai, V. Lefèvre-Seguin, and J. Hare, “Excitation mapping of whispering gallery modes in silica microcavities,” *Opt. Lett.* **35**, 583–585 (2010).
9. F. Orucevic, V. Lefèvre-Seguin, and J. Hare, “Transmittance and near-field characterization of sub-wavelength tapered optical fibers,” *Opt. Express* **15**, 13624–13629 (2007).
10. R. Bazzi, A. Brenier, P. Perriat, and O. Tillement, “Optical properties of neodymium oxides at the nanometer scale,” *J. Lumin.* **113**, 161–167 (2005).